Molecular alignment and filamentation: Comparison between weak- and strong-field models

N. Berti,[1,2] P. Béjot,[1,*] J.-P. Wolf,[2] and O. Faucher[1]

[1]*Laboratoire Interdisciplinaire CARNOT de Bourgogne, UMR 6303 CNRS-Université de Bourgogne, Boîte Postale 47870, 21078 Dijon, France*

[2]*Université de Genève, GAP-Biophotonics, Chemin de Pinchat 22, 1211 Geneva 4, Switzerland*

(Received 15 July 2014; published 26 November 2014)

The impact of nonadiabatic laser-induced molecular alignment on filamentation is numerically studied. Weak- and strong-field models of impulsive molecular alignment are compared in the context of nonlinear pulse propagation. It is shown that the widely used weak-field model describing the refractive index modification induced by impulsive molecular alignment accurately reproduces the propagation dynamics providing that only a single pulse is involved during the experiment. On the contrary, it fails at reproducing the nonlinear propagation experienced by an intense laser pulse traveling in the wake of a second strong laser pulse. The discrepancy depends on the relative delay between the two pulses and is maximal for delays corresponding to half the rotational period of the molecule.

DOI: 10.1103/PhysRevA.90.053851 PACS number(s): 42.65.Jx, 52.38.Hb, 34.50.Ez

I. INTRODUCTION

Since its first experimental observation in gases in the mid 1990s [1], laser filamentation, i.e., the nonlinear propagation of ultrashort intense laser pulses, has attracted extensive attention due to its physical interest, as well as its important applications including few-cycle optical pulse generation, terahertz generation, supercontinuum generation, and remote sensing [2–5]. The main feature of filamentation is its ability to sustain very high intensities (around 50 TW/cm^2) over very long distances in contrast with predictions of linear propagation theory. When exposed to such laser field intensities, atoms and molecules exhibit highly nonlinear dynamics leading to the observation of phenomena such as multiphoton and tunnel ionization, harmonic generation, and nonadiabatic molecular alignment. The last is a process that occurs when nonspherical molecules are exposed to a short and intense laser pulse [6]. The nonresonant interaction, driven by a pulse of duration much shorter than the classical rotational period, results in the production of postpulse transient molecular alignment revivals. The possibility of confining in space the rotational axes of a molecule, in the absence of the strong driving field, has been found particularly useful in various fields extending to high-harmonic generation and attosecond physics [7,8], molecular tomography [9,10], molecular-frame photoelectron angular distribution [11–13], control of molecular scattering [14], and more generally the study of direction-dependent interactions, to mention but a few. Moreover, field-free molecular alignment results in a modification of the local optical refractive index, which has been used for controlling the propagation dynamics of weak beams [15–17] and filaments [18–25]. Simulating laser pulse propagation over macroscopic distances in an aligned molecular medium is complicated by the need to include quantum-mechanical laser-molecule dynamics. While molecular alignment calculations are routinely performed with the time-dependent Schrödinger equation, its consideration in the context of two-dimensional laser propagation requires high numerical resources. Instead, the standard treatment of molecular alignment in propagation simulations consists of approximating the refractive index modification with a perturbation model, in which the rotational populations of the system remain unchanged upon the laser field application. In this approximation, the refractive index modification induced by molecular alignment is expressed as a convolution between the temporal pulse profile and the impulsive response of the molecule. This procedure provides a fast and efficient evaluation of the effect of molecular alignment that is convenient for laser propagation simulations. While this approximation is valid for the weak-field regime, the present work shows that it is no longer valid for intensities encountered in a filament, i.e., tens of TW/cm^2.

Nonlinear propagation simulations are compared using the weak-field model and the full quantum-mechanical treatment. Two cases can be distinguished. When a filament propagates through a thermal ensemble of molecules, the weak-field model reproduces well the full quantum simulation. On the contrary, when a filament propagates through an ensemble of molecules previously aligned by a second laser filament, the weak-field model fails at reproducing the propagation dynamics of the first filament. This is particularly the case when the delay between the two pulses matches the half-rotational period of the molecule [26,27].

This article is divided as follows. The first section is devoted to the refractive index modification induced by molecular alignment using the strong- and weak-field models. In the second section, numerical simulations of filamentation in molecular gases are performed using a strong-field modeling of molecular alignment. Their predictions are compared with those obtained with the "standard" weak-field model for the one- and two-pulse cases. It is shown that the weak-field model reproduces well the results obtained with the strong-field model in the case of a single filament. On the contrary, it fails at reproducing pump-pump experiments in which a laser filament propagates in the wake of a second filament.

II. MOLECULAR ALIGNMENT

A. Strong-field model

Laser-induced alignment of a molecular ensemble is described by solving the time-dependent Liouville

*pierre.bejot@u-bourgogne.fr

equation

$$i\frac{\partial}{\partial t}\varrho(t) = [H_{\rm rot} + H_{\rm int}(t), \varrho(t)], \tag{1}$$

where $[A,B] = AB - BA$ denotes the commutator operator, $\varrho(t)$ is the density matrix operator, and $H_{\rm rot} = B\mathbf{J}^2 - D\mathbf{J}^4$ is the rotational Hamiltonian, with $\mathbf{J}$ being the angular momentum and B (D) the rotational (centrifugal distortion) constant. For a linear molecule and a linearly polarized radiation, the interaction Hamiltonian is defined by

$$H_{\rm int} = -\tfrac{1}{4}\varepsilon(t)^2\Delta\alpha\cos^2\theta, \tag{2}$$

with $\Delta\alpha$ representing the polarizability anisotropy of the molecule and θ the angle between the molecule and the laser polarization axis [28]. The degree of molecular alignment with respect to the axis z is evaluated through both a quantum and a thermal averaging of the operator $\cos^2\theta$ as

$$\langle\langle\cos^2\theta\rangle\rangle = {\rm Tr}(\varrho\cos^2\theta), \tag{3}$$

where Tr defines the trace operator.

The refractive index modification $\Delta n_{\rm r}$ resulting from the molecular alignment is given by

$$\Delta n_{\rm r} = \frac{N\Delta\alpha}{2\epsilon_0}\langle\langle\cos^2\theta - 1/3\rangle\rangle, \tag{4}$$

with ϵ_0 being the permittivity of the vacuum and N the number density.

In the following, the initial density operator $\varrho(t=0)$ follows a thermal Boltzmann distribution taken at ambient temperature T. More particularly, the population $\varrho_0(J,M)$ for a state with quantum numbers J and M is

$$\varrho_0(J,M) = \frac{g_J e^{-\frac{E_{\rm rot}(J)}{k_{\rm B}T}}}{\sum_{J=0}^{\infty}(2J+1)g_J e^{-\frac{E_{\rm rot}(J)}{k_{\rm B}T}}}, \tag{5}$$

with $E_{\rm rot} = hc[BJ(J+1) - DJ^2(J+1)^2]$ being the energy of the rotational level, $k_{\rm B}$ the Boltzmann constant, and g_J the nuclear spin degeneracy factor.

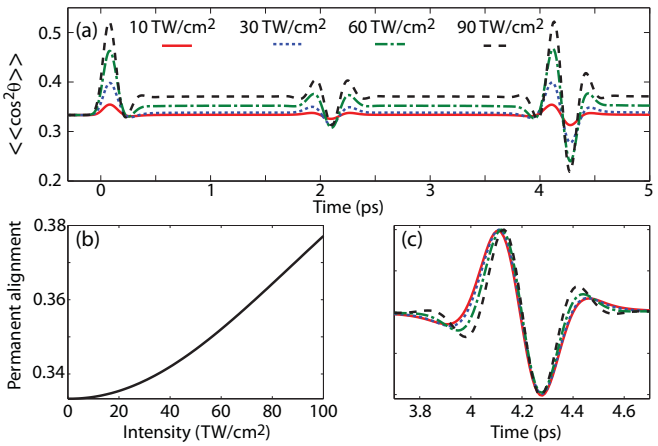

FIG. 1. (Color online) (a) Temporal evolution of the molecular alignment parameter $\langle\langle\cos^2\theta\rangle\rangle$ induced in N_2 at 300 K by a 100-fs pulse with different peak intensities. (b) Permanent alignment as a function of intensity. (c) First revival for different peak intensities.

As an example, Fig. 1(a) shows the alignment of N_2 calculated for different laser intensities. The molecular alignment can be split into two distinct components that differ by their temporal structures. The first one, called *alignment revival*, appears at each quarter of the rotational period $T_{\rm r}$. It results from the periodic rephasing of the rotational wave packet. The revival amplitude is proportional to the laser intensity in the weak-field regime, i.e., below 60 TW/cm^2 for nitrogen at room temperature. One has to emphasize that whereas the shape of the revivals is constant in the weak-field-regime approximation, the structural shape of the revival is no longer conserved when the field becomes stronger, as shown in Fig. 1(c). The second component, called the *permanent alignment*, comes from the population redistribution among rotational states. The interaction term defined in Eq. (2) only allows $\Delta J = 0$ and ± 2 and $\Delta M = 0$ transitions. Therefore, the result of the field action is to increase the total angular momentum J while its projection M remains constant. The permanent alignment is a direct consequence of the presence in the wave packet of the aligned rotational state with $J \gg M$. The permanent component becomes significant for an intense electric field and scales approximatively as the square of the laser intensity, as shown in Fig. 1(b).

B. Weak-field model

Calculation of two-dimensional propagation in laser-aligned molecules requires high numerical resources. To circumvent this problem, a standard approach consists of approximating the refractive index change induced by the molecular alignment with perturbation theory.

1. *Perturbation theory*

The perturbative expression of the nonlinear refractive index change induced by molecular alignment is evaluated as [29,30]

$$\Delta n_{\rm r}(t) = \frac{N\Delta\alpha^2}{15\hbar\epsilon_0^2 cn}\sum_J K_J {\rm Im}\left(e^{i\omega_J t}\int_{-\infty}^{t} I(t')e^{-i\omega_J t'}dt'\right), \tag{6}$$

where $I(t)$ is the laser intensity and K_J a factor defined by

$$K_J = g_J(\rho_{J+2} - \rho_J)\frac{(J+1)(J+2)}{2J+3}, \tag{7}$$

with ρ_J being the initial population of level J, g_J the nuclear spin degeneracy factor, c the speed of light, n the linear refractive index, and ω_J the Raman angular frequency between the J and $J+2$ levels. By defining the impulse response of the molecules $R(\tau)$ as

$$R(\tau) = \frac{N\Delta\alpha^2}{15\hbar\epsilon_0^2 cn}\Theta(\tau)\sum_J K_J\sin\omega_J\tau, \tag{8}$$

where $\Theta(\tau)$ is the Heaviside function, the change of refractive index can be obtained through a convolution with $I(t)$:

$$\Delta n_{\rm r} = R(t)I(t). \tag{9}$$

The knowledge of the impulse response R then allows one to evaluate the nonlinear refractive index change in the weak-field limit. Figure 2 displays the impulse response of air at ambient

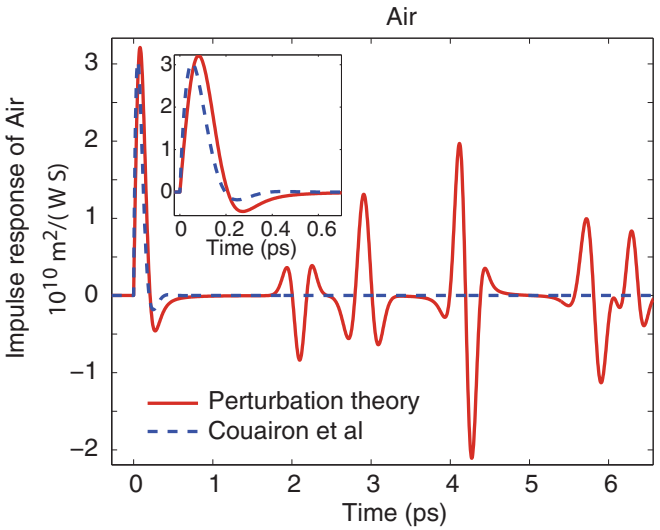

FIG. 2. (Color online) Impulse response of air at 300 K evaluated with the perturbation theory (red solid line) and the three-step model (blue dashed line).

conditions calculated within the weak-field framework. It has been obtained by adding the relative contributions of nitrogen and oxygen molecules.

2. *Three-level model*

The nonlinear refractive index can also be estimated by describing molecular alignment as a three-level nonresonant process [31], as depicted in Fig. 3. Δn_r is then evaluated through the differential equation

$$\frac{\partial^2 \Delta n_r}{\partial t^2} + 2\Gamma \frac{\partial \Delta n_r}{\partial t} + \Omega^2 \Delta n_r = \frac{\omega_r \mu^2}{\hbar^2 \Omega_0^2} |\varepsilon|^2, \qquad (10)$$

where μ is the transition dipole moment matrix element related to the transition energy $\hbar\Omega_0$, ω_0 is the angular frequency of the field ε, and $\Omega^2 = \omega_r^2 + \Gamma^2$, with ω_r being the Raman angular frequency and Γ a phenomenological dephasing rate. In the

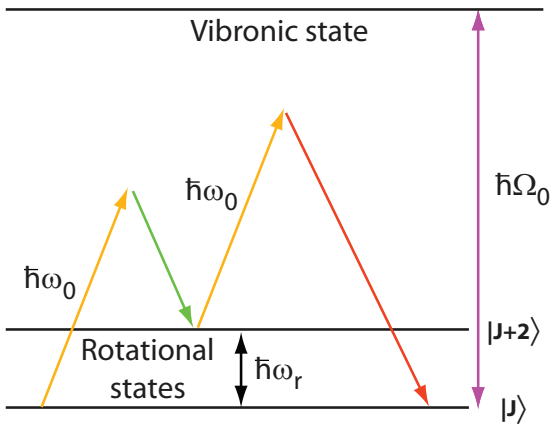

FIG. 3. (Color online) Three-level system used for the estimation of the rotational contribution to the nonlinear refractive index in the weak-field limit. The two populated rotational states J and $J+2$ are coupled through Raman-like transitions.

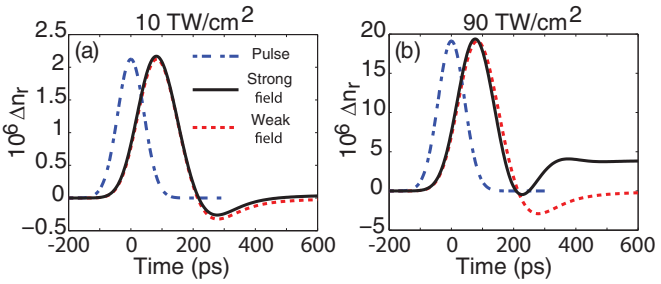

FIG. 4. (Color online) Nonlinear refractive index change induced by molecular alignment as a function of time evaluated by the weak (black solid lines) and the strong (red dashed lines) field theory for a 100-fs pulse. The peak intensity is (a) 10 TW/cm^2 and (b) 90 TW/cm^2.

frequency domain, the nonlinear refractive index $\widetilde{\Delta n}$ induced by the rotation is

$$\widetilde{\Delta n_r} = \frac{\omega_r \mu^2}{\hbar^2 \Omega_0^2} \frac{1}{\Omega^2 - \omega^2 + i2\Gamma\omega} \widetilde{|\varepsilon|^2} \qquad (11)$$

$$= \chi(\omega) \widetilde{|\varepsilon|^2}. \qquad (12)$$

In the temporal domain, the nonlinear refractive index is therefore described as in Eq. (9), where the impulse response $R(t)$ is written as

$$R(t) = \mathcal{R}_0 \Theta(t) \exp(-\Gamma t) \sin(\Omega t). \qquad (13)$$

The blue dashed curve in Fig. 2 shows the impulse response of air used in Ref. [4] and calculated according to Eq. (13). It is in qualitative agreement up to 500 fs with the response function calculated with Eq. (8). Even if this simplified model does not describe the periodic molecular alignment revivals, it remains so far the most widely used in filamentation simulations.

C. Molecular alignment: Weak field vs strong field

The alignment of N_2 at 300 K induced by a single 100-fs Gaussian pulse is investigated first. As shown in Fig. 4(a), the nonlinear refractive index calculated in the weak-field regime [Eq. (9)] is in good agreement with the strong-field calculation. For a larger intensity, as shown in Fig. 4(b), the discrepancy between the two models is due to the permanent alignment effect that is not taken into account in the perturbation theory. However, this contribution mainly affects the index after the field extinction, so that it only marginally impacts the pulse propagation dynamics. The weak-field theory is thus well suited for nonlinear propagation simulations in the case of a single pulse.

In the case of two delayed laser pulses, the molecular alignment can exhibit a complex dynamics. As already shown in Fig. 1(c), the weak-field approximation fails in reproducing both the deformation of the quantum revivals and the permanent alignment, which can have a large impact on a two-pulse experiment. Figure 5 depicts the nonlinear refractive index experienced by the second pulse evaluated either within the weak-field or the strong-field framework. Calculations have been performed for 100-fs (full width at half maximum) collinearly polarized pulses as a function of the peak intensity

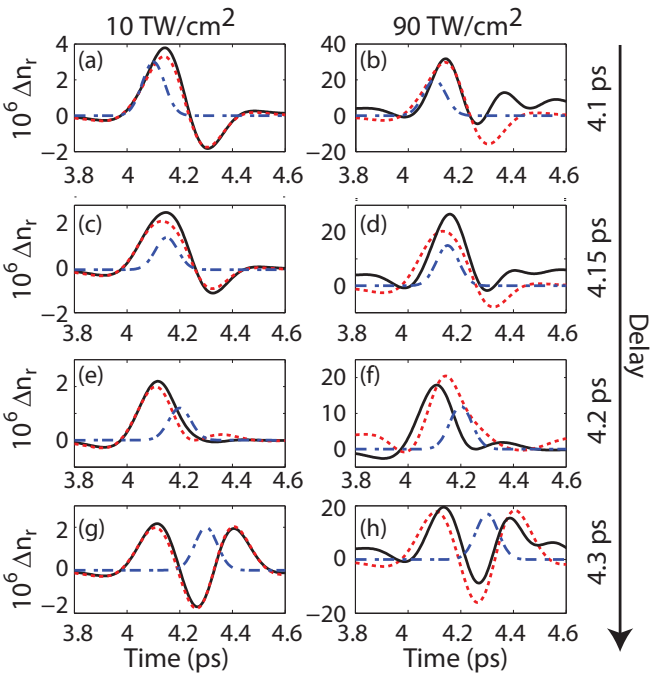

FIG. 5. (Color online) Temporal evolution of the nonlinear refractive index induced by molecular alignment evaluated by the weak-field theory (red dashed lines) and the strong-field theory (black solid lines) for different relative delays between the two pulses. The two pulses share the same peak intensity: 10 TW/cm^2 (left) and 90 TW/cm^2 (right). The dotted-dashed blue lines depict the probe pulse temporal intensity distribution.

and time delay. At low intensity (10 TW/cm^2), the permanent alignment is weak and the discrepancy between the two models remains marginal. This confirms that the perturbation framework is justified below this peak intensity value. It is clear that it does not apply at large intensity (90 TW/cm^2), where the discrepancy between the two models depends on the relative delay between the two pulses. As it is shown, the deviation of the weak-field model prediction is maximal at a delay corresponding to half the rotational period ($\simeq$4.2 ps).

III. IMPACT ON THE FILAMENTATION MODEL

A. Theory

Assuming a cylindrical symmetry around the propagation axis, the equation driving the propagation of a linearly polarized electric field envelope ε in the reciprocal space reads [32]

$$\partial_z \widetilde{\varepsilon} = i\left(k_z - \frac{\omega}{v_g}\right)\widetilde{\varepsilon} + \frac{\omega}{c^2 k_z}\left[i\omega(n_2|\widetilde{\varepsilon^2}\varepsilon + \Delta\widetilde{n_r\varepsilon}) - \frac{e^2}{2\epsilon_0 m_e}\zeta(\omega)\,\widetilde{\rho\varepsilon}\right] - \widetilde{L[\varepsilon]}, \quad (14)$$

where v_g is the group velocity; e (m_e) is the charge (mass) of the electron; $k_z = \sqrt{k^2(\omega) - k_\perp^2}$, with $k(\omega)$ being the wave vector and $k_\perp$ its transversal component; and $\zeta(\omega) = (\nu_{en} + i\omega)/(\nu_{en}^2 + \omega^2)$, with ν_{en} being the collision frequency between free electrons and neutrals atoms. The free-electron density ρ follows

$$\partial_t \rho = W(|\varepsilon|^2)(N - \rho) + \frac{\sigma}{U_i}|\varepsilon|^2 - g(\rho), \quad (15)$$

where $W(|\varepsilon|^2)$ describes the probability of ionization calculated with the PPT formula [33], σ is the inverse Bremsstrahlung cross section, U_i is the ionization potential, N is the numerical density of molecules, and g is the recombination function. An accurate modeling of the filamentation process would need to take into account the fact that the ionization process does depend on molecular alignment [34,35]. For instance, using our alignment calculations and the empirical formula derived by Litvinyuk *et al.* [36] that describes the ionization as a function of the angle between the molecule and the laser polarization axis, we estimated that the ionization in nitrogen increases by 33% (respectively decreases by 18%) if the latter is previously aligned (resppectively delocalized) by a 100-fs, 100 TW/cm^2 pulse. Nevertheless, the present work is devoted to pinpointing the limitation of the weak-field hypothesis for evaluating the nonlinear refractive index induced by the molecular alignment in the context of filamentation simulations. For the sake of simplicity, the alignment dependence of the ionization rate is disregarded.

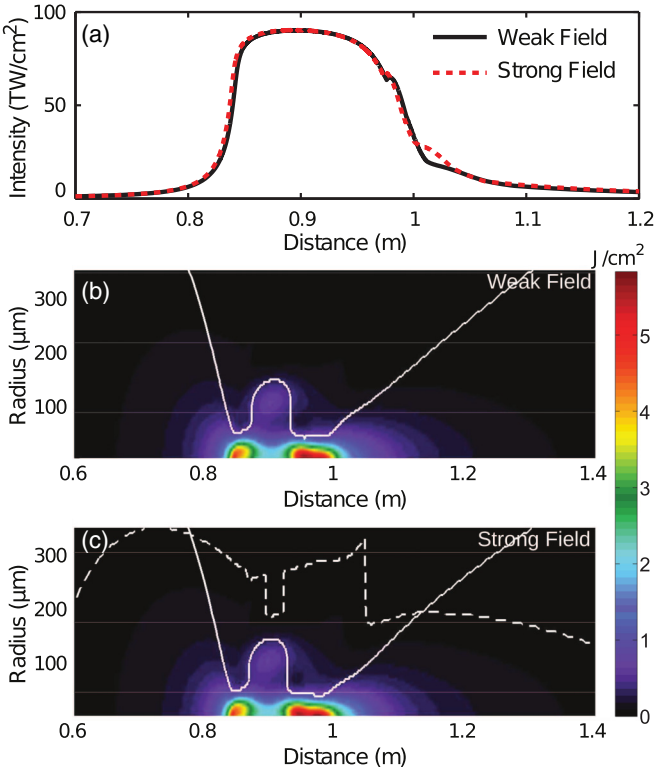

FIG. 6. (Color online) (a) Peak intensity as a function of the propagation distance of a single 100-fs pulse using the weak-field model (black solid line) and the strong-field model (red dashed line). Fluence distribution as a function of the propagation distance calculated with (b) the weak-field model and (c) the strong-field model. The white solid lines represent the radius of the beam and the white dashed line depicts the limit of strong-field calculations (see text).

The last term in Eq. (14) accounts for ionization-induced losses and is calculated as

$$L[\varepsilon] = \frac{U_i W(|\varepsilon|^2)}{2|\varepsilon|^2}(N - \rho)\varepsilon. \quad (16)$$

The change of refractive index induced by the molecular alignment is evaluated by using both the weak-field theory [Eqs. (8) and (9)] and the strong-field theory. In the latter, Eq. (1) was solved on spatial grid points where the pump fluence was higher than 0.05 J/cm^2, otherwise the weak-field model was used in order to reduce the computational time. Note that the convergence of the calculations was carefully checked by performing the strong-field calculations also for pump fluence higher than 0.02 J/cm^2.

B. Results and discussion

1. Single-pulse case

An 800-nm single pulse experiencing filamentation is considered. The 0.6-mJ 100-fs Gaussian pulse is focused with a 1-m focal length and propagates through gaseous nitrogen (4 bar, 300 K). The evolution of the on-axis intensity along the propagation is depicted in Fig. 6(a). The simulations are performed according to the strong- and weak-field models. In both cases, the nonlinear propagation model predicts a strong clamping of the intensity (around 90 TW/cm^2) induced by the dynamic equilibrium between the focusing and defocusing contributions to the refractive index. A slight deviation of the weak-field model from the strong-field prediction can be noticed at the falling part of the curves. As mentioned before, the strong-field calculations are limited to a spatial region where the pump fluence is larger than 0.05 J/cm^2. This limit is represented by the white dashed line in Fig. 6(c). As shown in Figs. 6(b) and 6(c), the weak field model also reproduces quite accurately the fluence distribution all along the propagation axis. These results confirm that the weak-field model is well suited for single-pulse simulations.

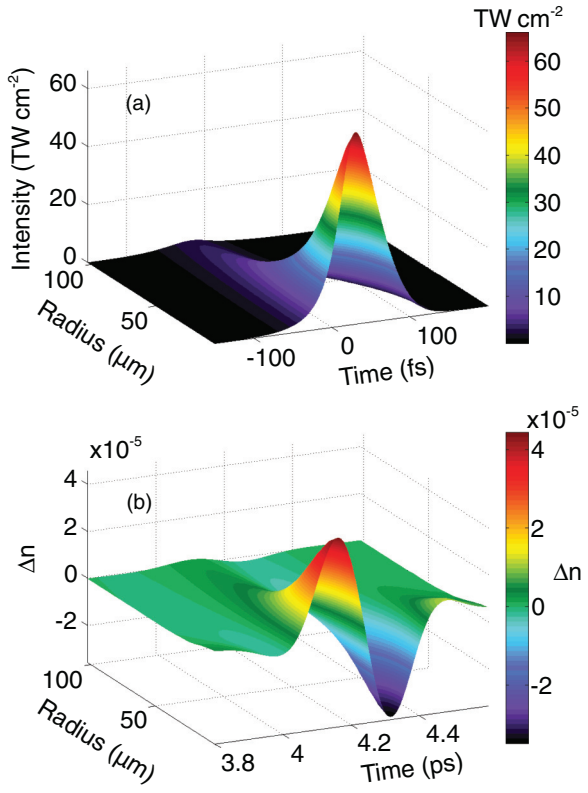

FIG. 7. (Color online) (a) Spatiotemporal intensity distribution of the pump at a propagation distance of 86 cm and (b) the associated nonlinear refractive index change induced by the latter. Depending on the delay between the pump and the probe, the former can induce either a focusing lens or a defocusing lens.

2. Double-pulse case

We now consider the filamentation dynamics of a pulse (denoted hereafter as a probe) traveling through a medium previously aligned by a second filament (denoted hereafter as a pump). The pump (probe) energy is 0.5 (0.6) mJ. Different relative delays between the pump and the probe beam are considered, so that the pump-induced molecular alignment acts as either a focusing or a defocusing lens, as depicted in Fig. 7. Note that the probe propagation dynamics without the pump correspond to the case depicted in Fig. 6. Depending on the relative delay between the pump and the probe beam, the position and length of the probe filament are differently affected. This depends on the sign of the nonlinear refractive

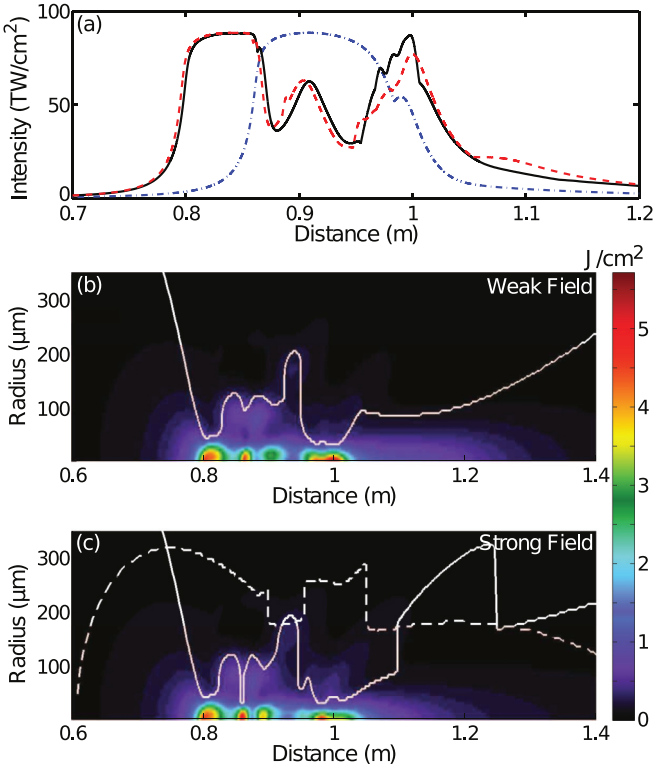

FIG. 8. (Color online) (a) Peak intensity along the propagation distance of the pump (blue dash-dotted line) and the probe evaluated with the weak-field theory (black solid line) and the strong-field theory (red dashed line). Panels (b) and (c) depict the probe fluence distribution along the propagation distance in the weak- and strong-field regimes, respectively. The white solid lines represent the radius of the beam and the white dashed line depicts the limit of strong-field calculations. The pump-probe delay is set to $\tau = 4.1$ ps.

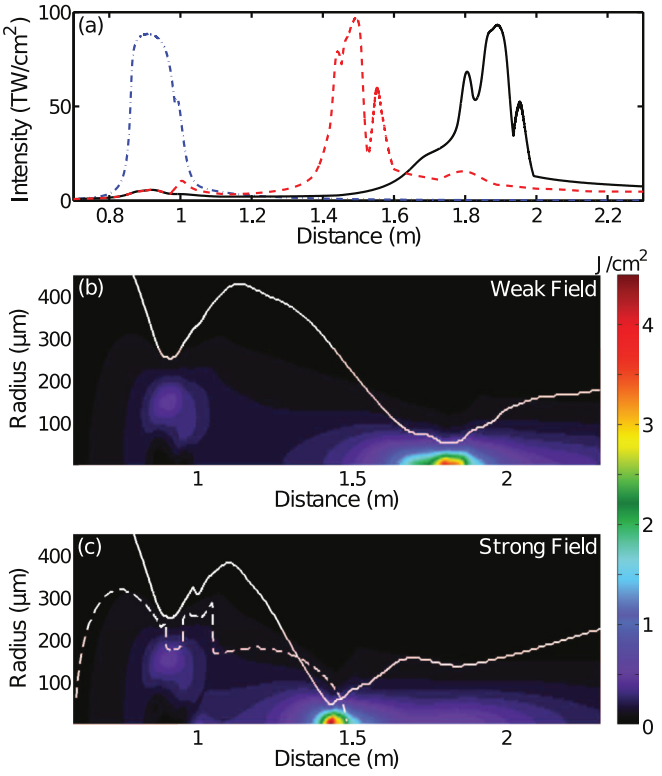

FIG. 9. (Color online) Same as Fig. 8 except for the pump-probe delay set to $\tau = 4.3$ ps.

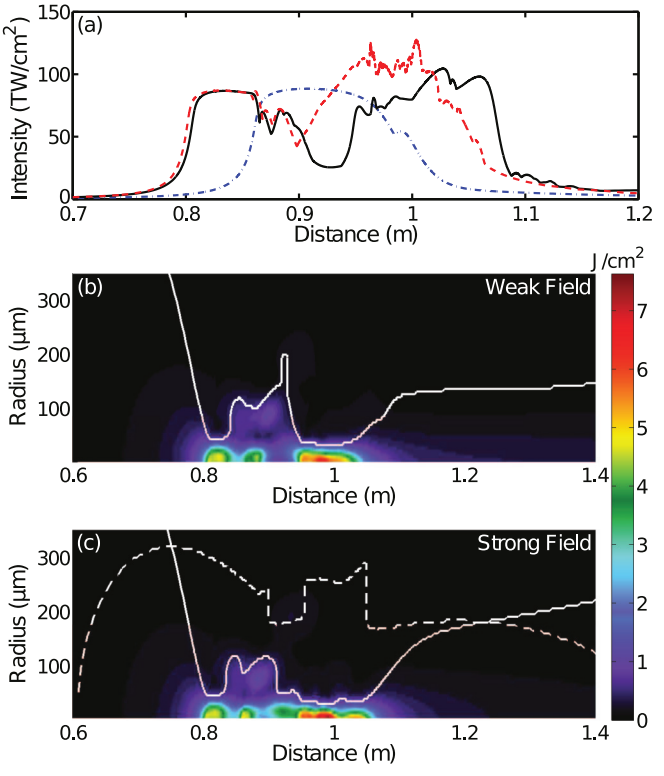

FIG. 10. (Color online) Same as Fig. 8 except for the pump-probe delay set to $\tau = 4.15$ ps.

index experienced by the probe, which is either positive, when the molecules are aligned, or negative, when they are delocalized around the field axis. For instance, the data presented in Fig. 8 correspond to a relative delay of $\tau = 4.1$ ps for which the pump-induced molecular alignment acts as a focusing lens ($\Delta n_r > 0$). In comparison to the single-pulse experiment, the probe filament sustains high intensities for a longer distance and its onset is shifted backward.

Note that the weak- and strong-field models predict very similar results in this case. This is consistent with the fact that the weak-field model accurately reproduces the nonlinear refractive index calculated at $\tau = 4.1$ ps [see Figs. 5(a) and 5(b)]. Figure 9 presents the same results but calculated for $\tau = 4.3$ ps. In that case, the pump-induced molecular alignment acts as a defocusing lens ($\Delta n_r < 0$), inducing a strong shift of the probe filament position. Moreover, Figs. 9(b) and 9(c) show that the predictions of both models completely differ at the quantitative level. For instance, the weak-field model predicts that the probe filament starts about 40 cm before the position predicted by the strong-field model. This discrepancy is due to the fact that the weak-field model fails at evaluating the nonlinear refractive index induced by molecular alignment at this particular delay [see Figs. 5(g) and 5(h)]. Similar disagreements are also reported at other delays lying around the half-rotational period, as shown, for instance, in Figs. 10 and 11. These results highlight the limit of the weak-field model and show that careful attention must be paid when evaluating the effect of molecular alignment on two-pulse experiments.

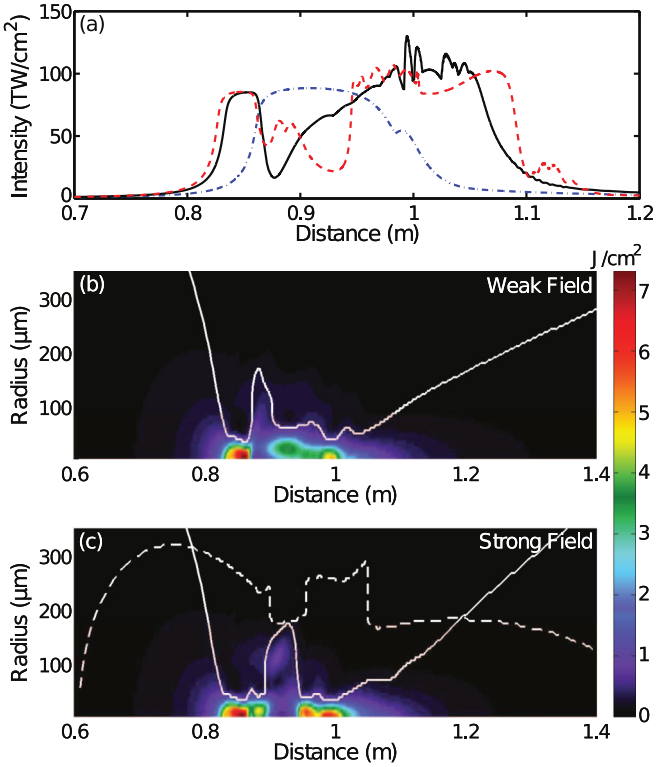

FIG. 11. (Color online) Same as Fig. 8 except for the pump-probe delay set to $\tau = 4.2$ ps.

IV. CONCLUSION

In this paper, the impact of molecular alignment on the propagation dynamics of a filament produced in a one- and two-pulse configuration is studied. For a single pulse, the weak-field model approximation provides a fair description of the refractive index change induced by molecular alignment. For a double pulse, i.e., when a probe filament propagates through a medium previously aligned by a pump filament, it is shown that the propagation dynamics of the latter is strongly influenced by the former, which acts as either a focusing lens or a defocusing lens, depending on the relative delay between the two pulses. At some specific delays, in particular when they lie around the half-rotational period of the molecule, the weak-field model is unable to capture the dynamics of the probe filament. This work therefore highlights the limit of weak-field calculations in filamentation simulations.

ACKNOWLEDGMENTS

This work was supported by the Conseil Régional de Bourgogne (PARI Program), the CNRS, the French National Research Agency (ANR) through the CoConicS Program (Contract No. ANR-13-BS08-0013), and the Labex ACTION Program (Contract No. ANR-11-LABX-0001-01). P.B. thanks the CRI-CCUB for the CPU loan on its multiprocessor server. J.-P.W. acknowledges financial support from the European Research Council Advanced Grant "Filatmo." The authors gratefully acknowledge E. Hertz for fruitful discussions. The assistance of M. Moret was highly appreciated.

[1] A. Braun, G. Korn, X. Liu, D. Du, J. Squier, and G. Mourou, Opt. Lett. **20**, 73 (1995).
[2] S. L. Chin, S. A. Hosseini, W. Liu, Q. Luo, F. Theberge, N. Aközbek, A. Becker, V. P. Kandidov, O. G. Kosareva, and H. Schroeder, Can. J. Phys. **83**, 863 (2005).
[3] L. Bergé, S. Skupin, R. Nuter, J. Kasparian, and J.-P. Wolf, Rep. Prog. Phys. **70**, 1633 (2007).
[4] A. Couairon and A. Mysyrowicz, Phys. Rep. **441**, 47 (2007).
[5] J. Kasparian and J.-P. Wolf, Opt. Express **16**, 466 (2008).
[6] H. Stapelfeldt and T. Seideman, Rev. Mod. Phys. **75**, 543 (2003).
[7] J. Itatani, D. Zeidler, J. Levesque, M. Spanner, D. M. Villeneuve, and P. B. Corkum, Phys. Rev. Lett. **94**, 123902 (2005).
[8] S. Haessler, J. Caillat, W. Boutu, C. Giovanetti-Teixeira, T. Ruchon, T. Auguste, Z. Diveki, P. Breger, A. Maquet, B. Carré, R. Taïeb, and P. Salieres, Nat. Phys. **6**, 200 (2010).
[9] J. Itatani, J. Levesque, D. Zeidler, H. Niikura, H. Pépin, J. C. Kieffer, P. B. Corkum, and D. M. Villeneuve, Nature (London) **432**, 867 (2004).
[10] M. Meckel, D. Comtois, D. Zeidler, A. Staudte, D. Pavičić, H. C. Bandulet, H. Pépin, J. C. Kieffer, R. Dörner, D. M. Villeneuve, and P. B. Corkum, Science **320**, 1478 (2008).
[11] C. Z. Bisgaard, O. J. Clarkin, G. Wu, A. M. D. Lee, O. Geßner, C. C. Hayden, and A. Stolow, Science **323**, 1464 (2009).
[12] L. Holmegaard, J. L. Hansen, L. Kalhøj, S. L. Kragh, H. Stapelfeldt, F. Filsinger, J. Küpper, G. Meijer, D. Dimitrovski, M. Abu-samha, C. P. J. Martiny, and L. B. Madsen, Nat. Phys. **6**, 428 (2010).
[13] J. L. Hansen, H. Stapelfeldt, D. Dimitrovski, M. Abu-samha, C. P. J. Martiny, and L. B. Madsen, Phys. Rev. Lett. **106**, 073001 (2011).
[14] E. Gershnabel and I. S. Averbukh, Phys. Rev. Lett. **104**, 153001 (2010).
[15] F. Calegari, C. Vozzi, S. Gasilov, E. Benedetti, G. Sansone, M. Nisoli, S. De Silvestri, and S. Stagira, Phys. Rev. Lett. **100**, 123006 (2008).
[16] H. Cai, J. Wu, A. Couairon, and H. Zeng, Opt. Lett. **34**, 827 (2009).
[17] Y. Wang, X. Dai, J. Wu, L. Ding, and H. Zeng, Appl. Phys. Lett. **96**, 031105 (2010).
[18] J. Wu, H. Cai, H. Zeng, and A. Couairon, Opt. Lett. **33**, 2593 (2008).
[19] Y. Peng, H. Cai, J. Wu, and H. Zeng, Opt. Express **17**, 5822 (2009).
[20] J. Wu, H. Cai, Y. Peng, Y. Tong, A. Couairon, and H. Zeng, Laser Phys. **19**, 1759 (2009).
[21] J. Wu, H. Cai, Y. Peng, and H. Zeng, Phys. Rev. A **79**, 041404 (2009).
[22] F. Calegari, C. Vozzi, and S. Stagira, Phys. Rev. A **79**, 023827 (2009).
[23] H. Cai, J. Wu, X. Bai, H. Pan, and H. Zeng, Opt. Lett. **35**, 49 (2010).
[24] S. Varma, Y.-H. Chen, J. P. Palastro, A. B. Fallahkair, E. W. Rosenthal, T. Antonsen, and H. M. Milchberg, Phys. Rev. A **86**, 023850 (2012).
[25] J. P. Palastro, T. M. Antonsen, Jr., S. Varma, Y. H. Chen, and H. M. Milchberg, Phys. Rev. A **85**, 043843 (2012).
[26] M. Lapert, E. Hertz, S. Guérin, and D. Sugny, Phys. Rev. A **80**, 051403 (2009).
[27] Md. Z. Hoque, M. Lapert, E. Hertz, F. Billard, D. Sugny, B. Lavorel, and O. Faucher, Phys. Rev. A **84**, 013409 (2011).
[28] A. Rouzée, E. Hertz, B. Lavorel, and O. Faucher, J. Phys. B **41**, 074002 (2008).
[29] M. Morgen, W. Price, L. Hunziker, P. Ludowise, M. Blackwell, and Y. Chen, Chem. Phys. Lett. **209**, 1 (1993).
[30] C. H. Lin, J. P. Heritage, T. K. Gustafson, R. Y. Chiao, and J.-P. McTague, Phys. Rev. A **13**, 813 (1976).
[31] J. R. Penano, P. Sprangle, P. Serafim, B. Hafizi, and A. Ting, Phys. Rev. E **68**, 056502 (2003).
[32] M. Kolesik and J. V. Moloney, Phys. Rev. E **70**, 036604 (2004).
[33] A. M. Perelomov, V. S. Popov, and M. V. Terentev, Sov. Phys. JETP **23**, 924 (1966).
[34] Z. X. Zhao, X. M. Tong, and C. D. Lin, Phys. Rev. A **67**, 043404 (2003).
[35] D. Pavicic, K. F. Lee, D. M. Rayner, P. B. Corkum, and D. M. Villeneuve, Phys. Rev. Lett. **98**, 243001 (2007).
[36] I. V. Litvinyuk, K. F. Lee, P. W. Dooley, D. M. Rayner, D. M. Villeneuve, and P. B. Corkum, Phys. Rev. Lett. **90**, 233003 (2003).